Available online at www.sciencedirect.com
ScienceDirect
Icarus 190 (2007) 334–344
ICARUS
www.elsevier.com/locate/icarus

Evolution of the Deep Impact flash: Implications for the nucleus surface based on laboratory experiments

Carolyn M. Ernst *, Peter H. Schultz

Department of Geological Sciences, Brown University, Providence, RI 02912-1846, USA

Received 1 September 2006; revised 10 March 2007

Available online 24 April 2007

Abstract

The Deep Impact flyby spacecraft obtained high-speed images of the evolving impact event. Multiple exposures captured a self-luminous impact flash, caused by the heating and vaporization of the cometary surface. Laboratory investigations show that target conditions affect the photometric and spatial evolutions of the impact flash; thus, the flash can be used to constrain the state of the target if the other initial impact conditions are known. Through comparisons of DI flash observations to laboratory impact experiments, the impact flash evolution can be used to determine the type of impact that occurred and to interpret the nature of the impacted Tempel 1 surface. The Deep Impact flash was of relatively long duration, though its luminous efficiency was an order of magnitude lower than expectations. Both uprange and downrange self-luminous plumes were observed. Comparisons of the DI observations with the results of laboratory experiments suggest that the surface of Tempel 1 contains silicates, volatiles, and carbon compounds, and is a highly-porous substrate.

Keywords: Comet Tempel-1; Comets; Cratering; Impact processes

1. Introduction

The NASA Deep Impact (DI) mission performed a planetary-scale impact into Comet 9P/Tempel 1 on July 4, 2005 at 05:44:36 UTC. The mission was designed to explore the structure and composition of a cometary nucleus by observing the impact event. The impact conditions were well known and controlled, as they are in laboratory experiments: a 370 kg impactor (49% copper by weight) impacted the comet at 10.3 km s^{-1}, delivering ~20 GJ of energy to the nucleus (A'Hearn et al., 2005). The impact was oblique, occurring at an angle between 25° and 35° (measured from the horizontal) as determined by flyby spacecraft images, a derived shape model (Thomas et al., 2007), and the foreshortening of circular features (A'Hearn et al., 2005). Many phenomena can be used to analyze and assess various aspects of an impact in order to interpret the event and to constrain or determine any unknown conditions. In the case of the Deep Impact experiment, the major unknown was the state of the target: the Tempel 1 nucleus. The impact flash is one phenomenon that can be used to place constraints on the nucleus structure.

Hypervelocity impacts induce heating and vaporization in both the projectile and the target. Assuming the heated material radiates as a blackbody, the emitted energy follows a universal wavelength spectrum. The total energy partitioned to the target increases with the initial kinetic energy of the projectile, resulting in higher material temperatures.

Wien's law states that the wavelength at which the maximum specific intensity is radiated (λ_{max}) is inversely proportional to the temperature (T):

$$\lambda_{max} = \frac{b}{T}, \tag{1}$$

where b is the Wien displacement constant. At high enough temperatures, the radiated light includes wavelengths in the visible range (as well as in the infrared and, if hot enough, the ultraviolet) that can be detected with instruments sharing the spectral response range of the human eye. This visible radiation is known as the "impact flash."

* Corresponding author. Fax: +1 (401) 863 3978.
E-mail address: carolyn_ernst@brown.edu (C.M. Ernst).

0019-1035/$ – see front matter
doi:10.1016/j.icarus.2007.03.030

The impact flash is a well-documented phenomenon that has been observed during natural impacts as well as during laboratory impact experiments. Several studies have documented light flashes caused by meteoroid impacts into the Moon (e.g., Bellot Rubio et al., 2000a, 2000b; Ortiz et al., 2000, 2002; Yanagisawa and Kisaichi, 2002) and in a more extreme (and more complicated) case by the Shoemaker–Levy 9 impacts into Jupiter's atmosphere (e.g., Zahnle and MacLow, 1995). These impacts were natural events, which are difficult to observe and are rare occurrences. In both the lunar meteoroid and Shoemaker–Levy 9 cases, the major unknown initial conditions were the projectile properties (e.g., size, composition). The Shoemaker–Levy 9 flash, however, was an atmospheric entry phenomenon.

The impact flash has been studied extensively in laboratory settings, where initial conditions can be controlled, repeated, and systematically varied. Previous studies quantified the effect of impact velocity, angle, projectile diameter, and projectile and target composition on the resulting flash and derived relationships between the initial conditions and the resulting impact flash peak intensity, temperature, duration, and luminous efficiency (e.g., Gehring and Warnica, 1963; Eichhorn, 1976; Kadono and Fujiwara, 1996; Ernst and Schultz, 2002, 2003, 2004, 2005).

Experimental impacts into particulate silicate targets produce prolonged impact flashes that last orders of magnitude beyond the time it takes the projectile to penetrate the target (Ernst and Schultz, 2003). In these experiments, the impact heats the particulates, which act as blackbody radiators that cool over time. Most of the heated particulates remain inside of the developing crater, either lining the cavity or being buried within the target. At later times, some heated material leaves the impact site as ejecta. If volatiles are introduced into the original target, heated particulates can be entrained inside of the evolving vapor plume. In the case of an oblique impact, this plume can transport the radiating particulates downrange of the impact site (Schultz, 1996; Schultz et al., 2006).

Experimental impacts demonstrate that the observable photometric and spatial evolutions of an impact flash are highly dependent on initial conditions. The initial kinetic energy of the projectile, the impact angle, and the target properties (e.g., porosity, composition) have significant and observable influences on the magnitude and evolution of the impact flash. Because of these dependences, laboratory-derived relationships can be used to predict the evolution of an impact flash for given impact conditions. Alternatively, analysis of the impact flash evolution allows unknown conditions to be constrained when most of the initial conditions are known.

Despite the strengths of laboratory settings, laboratory impact experiments cannot achieve the full range in size, speed, and gravitational conditions of natural impacts. For this reason the DI collision was a novel experiment, occurring at large scales outside of a laboratory while most of the initial conditions were controlled. Because DI is the first experiment of its kind, there are no similar experiments for comparison. Thus, laboratory impact studies are essential for understanding the DI event in particular, and impact processes in general.

The duration of an impact flash depends on initial conditions, especially the scale of the event (velocity, size). The afterglows from laboratory impact flashes can last as long as ∼2 ms for macroscopic impacts into particulate silicate targets (Ernst and Schultz, 2003), whereas lunar meteoroid impact flashes have been observed for as long as 600 ms (Ortiz et al., 2002). All other conditions being the same, larger-scale events are expected to produce longer-duration flashes due to the greater mass of heated target material. The large scale of the DI event means the entire cratering processes, including the impact flash duration, will operate on a longer timescale than in the laboratory.

One method of scaling the timescale of the event is to relate the time after impact (t) to the penetration of the projectile (the time it takes the projectile to travel its diameter into the target):

$$\tau = \frac{t}{(a/v)}, \tag{2}$$

where a is the projectile diameter and v is the impact velocity (Schultz et al., 2005). Whereas the flash typically lasts ∼2 ms, or $\tau \sim 2000$, for the current impact experiments, the same flash would last significantly longer at DI size and velocity scales (assuming all other initial conditions are the same), where $\tau = 2000$ is equivalent to a time of ∼2000 ms.

In this paper we investigate the photometric and spatial evolutions of the DI flash based on images taken by the flyby spacecraft. We compare the DI flash to experimental results in order to interpret the event. Comparisons of the spacecraft observations with the Schultz et al. (2005) pre-mission predictions help to assess the validity of extrapolations based on laboratory experiments and to evaluate the differences between the laboratory impacts and the Deep Impact collision. Our results include the calculation of the luminous efficiency of the DI flash, as well as interpretations of the impact event and implications for the nature of the Tempel 1 surface.

2. Deep Impact observations

Two instruments onboard the DI flyby spacecraft observed the impact event, the Medium Resolution Instrument (MRI) and the High Resolution Instrument (HRI). Though having a lower spatial resolution, the MRI images had a much shorter time resolution than the HRI images during and immediately after the moment of impact (59 ms versus ∼840 ms) and provide the only data on the flash evolution. The MRI consists of a filtered visible-light CCD camera (0.32–1.05 μm) connected to a telescope with a 12 cm aperture and a 2.1 m focal length (Hampton et al., 2005). The image sequence recorded from $I - 0.5$ s to $I + 1.0$ s (where I is the expected time of impact) was designed to capture the initial stages of the impact event at the fastest possible time resolution (59 ms) and at a spatial resolution of 86 m/pixel (Klaasen et al., 2005). The sampling rate encompassed a 51.4 ms exposure plus 7.6 ms for data readout. The separation angle between the flyby spacecraft's view of the impact point and the impactor itself was 3.3°, resulting in a highly oblique view angle of the impact event (very close to the angle of impact). Fig. 1 is a composite image of the Tempel 1

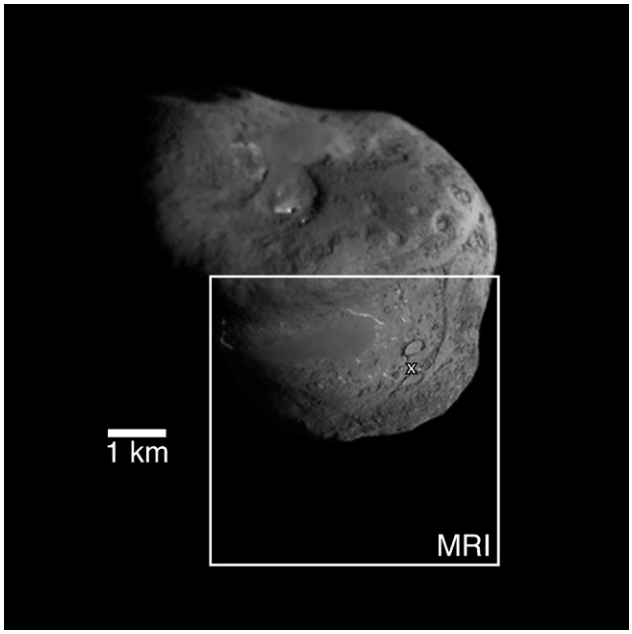

Fig. 1. The Tempel 1 nucleus. This is a composite of the best impactor targeting sensor (ITS) images. The Sun is to the right. The box indicates the MRI field of view at the time of impact. The impact point is indicated by the white "x."

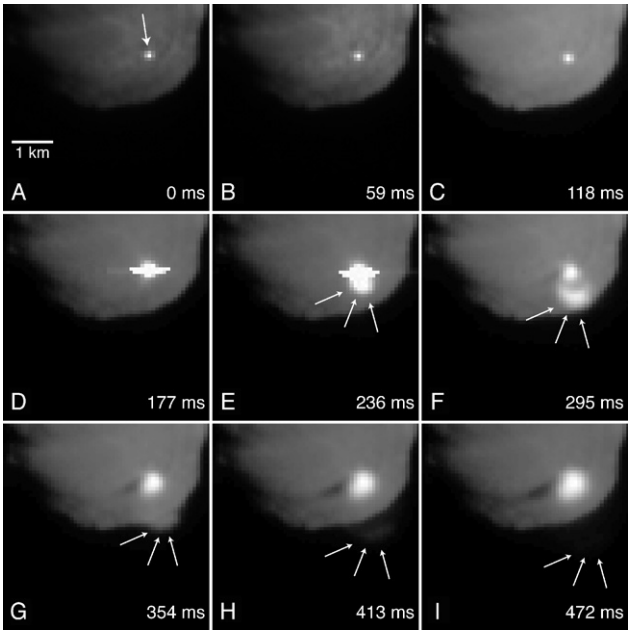

Fig. 2. The first nine post-impact MRI images (out to $\sim I + 500$ ms). The listed times are the exposure start times with respect to the "first light" signal (frame A). The initial first light signal was overtaken by a delayed bright (saturated) signal after 117 ms (frame D). A vapor plume emerged and expanded downrange, away from the impact site, beginning in frame E. The arrow in frame A indicates the projected impact trajectory, and those in frames E–I indicate the expanding vapor plume.

nucleus, composed of the best images taken by the impactor targeting sensor (ITS) on board the impactor spacecraft. The box indicates the MRI field of view at the time of impact. The entire evolving impact flash remained within the MRI field of view.

Multiple MRI exposure frames captured the impact flash produced by the DI collision. The flash evolved most dramatically over the first nine post-impact MRI images (exposure IDs 9000910_064-072), which cover the first ∼530 ms after impact and are depicted in Fig. 2. The labeled post-impact times are with respect to the "first light" (first flash appearance) in the exposure started at 05:44:36 UTC (frame A).

The MRI exposure sequence introduces small uncertainties when analyzing the evolution of the impact flash. The changes to the flash within an exposure cannot be determined. Though not a significant concern at later times, at early times the impact flash evolved rapidly with respect to the time resolution of the MRI, making it more difficult to interpret the flash evolution. Similarly, the "first light" signal could have appeared at any point during the frame A exposure. Another issue is the 7.6 ms time gap between exposures when the comet was not being imaged. The absence of these data results in further uncertainty, especially when there appear to be large discontinuities in the photometric evolution (e.g., between frames C and D, and between frames D and E). The saturation of the detector also leads to uncertainty, as any measured saturated value must be considered as a minimum. Despite the uncertainties inherent to the exposure sequence, the MRI images contain sufficient information to determine the photometric and spatial evolutions of the impact flash. The following overview of the phenomenology contains some interpretations based on analyses that will be described later in the text.

2.1. Deep Impact flash intensity overview

The "first light" was relatively small and dim and was mostly confined to one pixel (frame A in Fig. 2). A delayed brightening began by ∼118 ms (frame C), after which the light intensity quickly increased to the point of detector saturation (frame D), leading to the horizontal charge bleeding seen in frames D and E. As the bright flash evolved further, a luminous plume appeared and expanded downrange, away from the point of impact. The leading edge of the plume can be easily seen in frames E–G (and is indicated by arrows in frames F–I). Both the early central portion of the light signal (consisting of the first light, the delayed brightening, and the saturated signals) and the downrange plume were self-luminous and make up what is considered to be the impact flash.

A second light source emerged from the impact point by 295 ms (frame F) and grew in both area and intensity during subsequent exposures. The source of this light was sunlight reflecting off of the expanding central ejecta cloud. Since this source was not self-luminous, it is not considered to be a part of the impact flash; if the impact had occurred on the dark side of the nucleus, the MRI would not have observed this component. The ejecta cloud casts a shadow onto the nucleus, which is first visible in frame F. The existence of the shadow indicates that at this time (295 ms after impact) the reflecting ejecta cloud was optically thick.

In contrast to the ejecta cloud, none of the impact flash components cast observable shadows onto the nucleus. This could imply that these components were optically thin, though it is possible that these components had strong enough self-

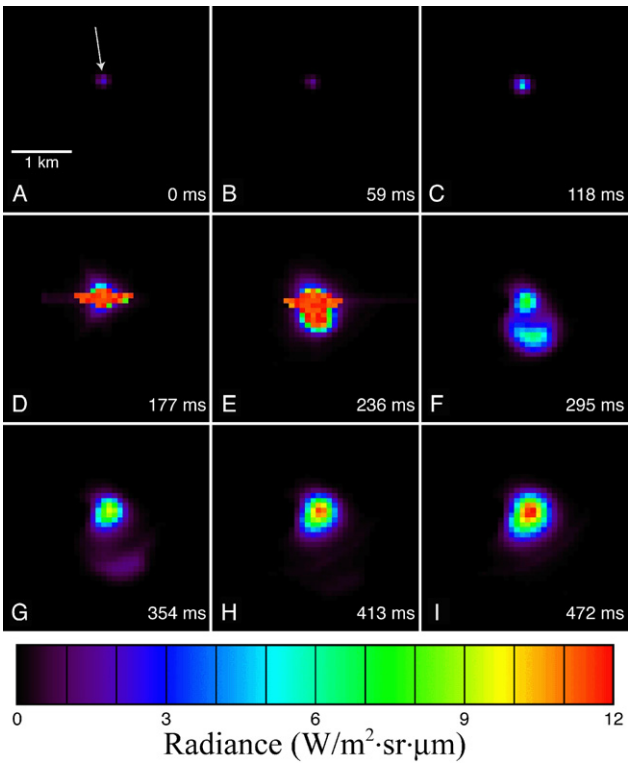

Fig. 3. An alternate display of the first nine post-impact MRI images. The multi-color scale better highlights details in the light intensity. The frames correspond to zoomed-in views of those in Fig. 2. A pre-impact image was subtracted from each post-impact MRI image in order to remove non-impact related light sources (including sunlight reflecting off of the nucleus surface).

luminosity to illuminate the surface, eliminating a potential shadow. Based on preliminary modeling, Melosh et al. (2006) state that the downrange luminous plume was optically thin in all images with the possible exception of its first appearance (frame D).

Fig. 3 depicts the photometric and spatial evolution of the impact flash in a false-color representation in order to better view intensity variations. Here, the color scale corresponds to the intensity of the recorded light signal. The frames correspond to a zoomed in view of those in Fig. 2, and the arrow in frame A represents the direction of impact. The final pre-impact MRI image (9000910_063) was subtracted from each post-impact MRI image in order to remove non-impact related light sources (including sunlight reflecting off of the nucleus surface).

2.2. *Photometric evolution*

Two light source components associated with the impact were observed: an early-time self-luminous source (the impact flash) and a later-time, reflected-light source (the expanding ejecta cloud). Fig. 4 shows the evolution of the spatially integrated DI light intensity through time with respect to the appearance of the first light (displayed as the cumulative intensity of a given component for each MRI exposure). The MRI CCD has a linear response; so, the bleed-over light from each of the two saturated frames (D and E) was summed to determine the minimum total brightness for these exposures.

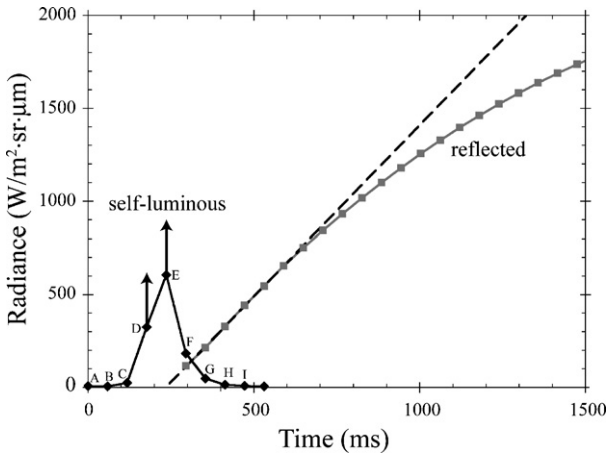

Fig. 4. Plot of the light intensity evolution of the first 1500 ms of the Deep Impact collision. The black curve represents the self-luminous (impact flash) portion of the light output. The intensity values for the saturated images represent minimum values. The gray curve represents the light reflected off of the expanding ejecta cloud. The dashed line is the initial linear growth trend of the reflecting portion extrapolated through time. The letters correspond to those from Fig. 2.

The self-luminous component on the graph represents the impact flash, consisting of the light flux spatially integrated over not only the central "first light" (A, B) and delayed brightening (C–E), but also the expanding downrange plume (E–I). The overall photometric evolution began as a faint signal that faded before quickly and dramatically undergoing a delayed brightening, bringing the signal beyond the level of detector saturation. After this point, the signal slowly decayed. The primary light source for the impact flash component is thermal radiation from heated and melted ejecta particulates. The intensity of the entire central reflected-light portion of the light signal initially underwent linear growth (beginning in frame F, 295 ms), but by ∼650 ms after impact its growth began to slow, diverging from this linear trend.

2.3. *Spatial evolution*

The center of brightness of the impact flash moved over the first ∼175 ms after impact. In order to examine this movement, center of brightness positions from successive MRI exposures (corresponding to frames A–D of Fig. 2) were resized and overlain onto a deconvolved HRI/ITS composite image of the nucleus (Fig. 5). Fig. 5 contains the overlay of the entire nucleus as a context image, as well as a zoomed-in view of the impact site and surrounding region.

The projected movement of the flash was along a line lying at an angle to the impactor trajectory, i.e., not along a surface tangent. The center of brightness of the "first light" signal (A) occurred one pixel uprange from the location of the delayed brightening in frame C (∼100–200 m, taking into account the oblique view angle). This delayed signal was located another 100–200 m uprange from the center of brightness of the first saturated image (D). The movement between frames C and D was likely due to the initial downrange emergence from the impact site of the plume containing hot vapor, gas, and entrained

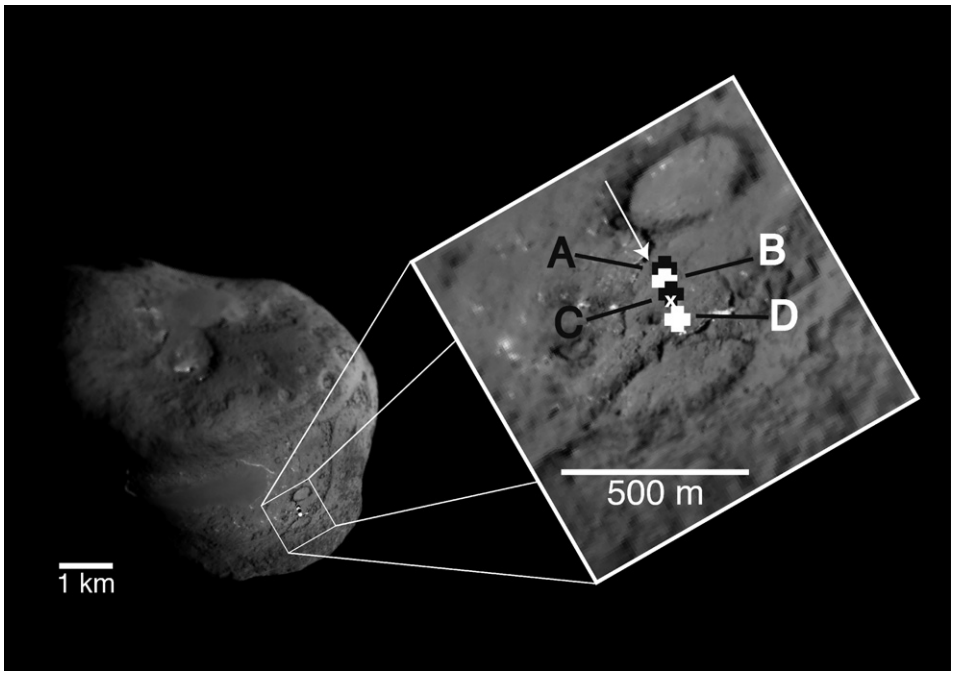

Fig. 5. Movement of the impact flash at early times, illustrated by the location of the center of brightness for a given MRI exposure. The letters correspond to the exposure frames from Fig. 2: (A) represents the center of brightness of the first light, (C) represents the beginning of the delayed brightening (100–200 m downrange of the first light), and (D) represents the center of brightness of the first saturated exposure (located another 100–200 m downrange). The projected impact point is indicated by an "x." The arrow represents the projected impact trajectory, and lies at an angle to the apparent movement of the flash. The background image is a subset of the comet surface as observed by the impactor spacecraft (ITS) before the impact. The nucleus context image is a composite of the best ITS images.

particulates. The movement between A and C was due to a more complex process, which will be explored, with input from laboratory experiments, in Section 4.

3. Experimental results

The Deep Impact collision was a one-of-a-kind impact event: most of the variables were controlled as in laboratory experiments, but the impact occurred at planetary scales. The possible outcomes of the collision were explored through the use of laboratory analogs to DI conditions. By comparing and contrasting photometric and spatial characteristics of laboratory impact flashes and DI observations, we can place constraints on the type of impact that occurred and the nature of the Tempel 1 nucleus surface.

The DI impact velocity was only about twice that typically achieved by experiments (10.3 versus ∼5.5 km s^{-1}); however, the DI projectile was ∼10^6 times more massive (370 kg versus 0.30 g). Together, these scale differences translate to an initial DI kinetic energy ∼4×10^6 times larger than typical laboratory kinetic energies (20 GJ versus 5 kJ). The great difference in projectile kinetic energy introduces challenges when scaling the laboratory results to DI conditions. For example, with so much more energy available, some materials will vaporize that otherwise would remain in solid or liquid form. Other challenges arise since the materials used in experiments are not the same as those found on a cometary surface.

To address these challenges, various targets were chosen for their specific characteristics: pumice dust (non-volatile, silicate, particulate), solid pumice block (strength), perlite granules (high porosity), dolomite (easily vaporizable under laboratory conditions), and sugar (carbonaceous composition). These target materials were not used to reproduce the surface of Tempel 1; rather, they are surrogates used to assess the effect of their specific properties on the resulting light signal.

3.1. Target effects on impact flash photometric characteristics

The peak intensity, duration, and luminous efficiency of an impact flash are all easily observable photometric characteristics that are greatly affected by target properties. The luminous efficiency of an impact (η) is the fraction of the initial kinetic energy (KE_o) emitted as luminous energy (LE) over a given wavelength (λ_1 to λ_2) when an impact occurs:

$$\int_{\lambda_1}^{\lambda_2} LE = \eta KE_o. \tag{3}$$

We consider the luminous efficiency over a primarily visible wavelength range for this study, since the MRI observed the Deep Impact collision from 0.32 to 1.05 μm.

In practice, not all of the light generated by an impact will be observable by a detector above the surface, thereby affecting the observed luminous efficiency. During laboratory impact experiments, some of the emitting material can be buried in the target or obscured by other ejecta. In addition, the developing transient crater can prevent radiating material from being exposed at the surface. The degree to which the obscuration occurs relates to the nature of the target and the impact angle. For example, obscuration by the transient crater becomes

Table 1
Experimental target properties

Target	Composition	ρ_b (g cm^{-3})	ρ_p (g cm^{-3})	ϕ
Pumice powder	Rhyolitic (>70% SiO_2)	1.25	2.20	0.43
Sieved perlite granules	Rhyolitic	0.22	2.20	0.90
Solid pumice block	Rhyolitic	0.62	2.20	0.72
Sugar	$C_{12}H_{22}O_{11}$	0.97	1.58	0.39
Dolomite powder	$CaMg(CO_3)_2$	1.33	2.85	0.53

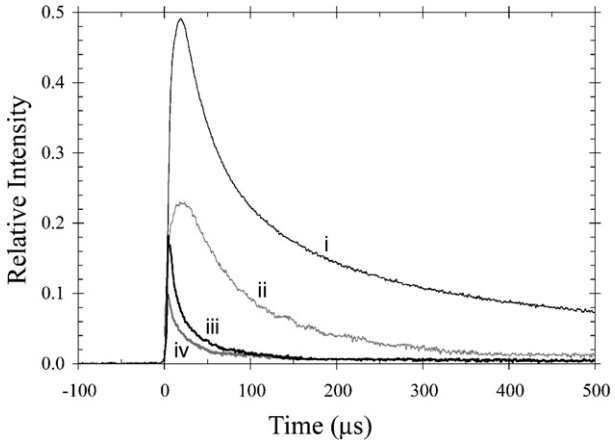

Fig. 6. Plot of the light intensity evolution of experimental impacts into targets of different porosity and volatile content. Both increasing porosity [seen in the difference between the pumice powder (a), solid pumice (b), and perlite granule (c) targets] and increasing volatile content [seen in the difference between the pumice powder (a) and dolomite powder (d) targets] lead to a suppression of the luminous output of an impact.

more pronounced in the case of a high-porosity target, where the transient crater is extremely narrow and deep before eventually opening and exposing its contents at the surface (Schultz et al., 2005).

Experimental impacts were performed at the NASA Ames Vertical Gun Range to explore the effects of target porosity and composition on the resulting impact flash. In order to minimize the number of variables, target type was the only initial condition changed. The impact velocity for all of the experiments described in this section was 5.67 ± 0.16 km s^{-1}, and the impact angle remained constant at 30° from the horizontal. All projectiles were 0.635 cm-diameter Pyrex spheres. At these velocities, Pyrex disrupts completely on impact, thus better simulating conditions met during larger-scale impacts (Schultz and Gault, 1990). All of the experiments in this study took place under near-vacuum conditions (<0.72 mbar). At these very low pressures, the residual atmosphere does not affect the brightness or the evolution of the flash (Ernst and Schultz, 2004).

Materials of similar particulate silicate composition were used to vary the target porosity from as low as 43% (pumice powder, 81 μm mean grain size) to as high as 90% (perlite granules, sieved to <500 μm). Table 1 contains the composition and porosity for all of the target materials used in this study. The effect of target porosity on the impact flash evolution can be seen in Fig. 6. As the porosity increases, the peak intensity, overall impact flash brightness, and duration decrease, resulting in a

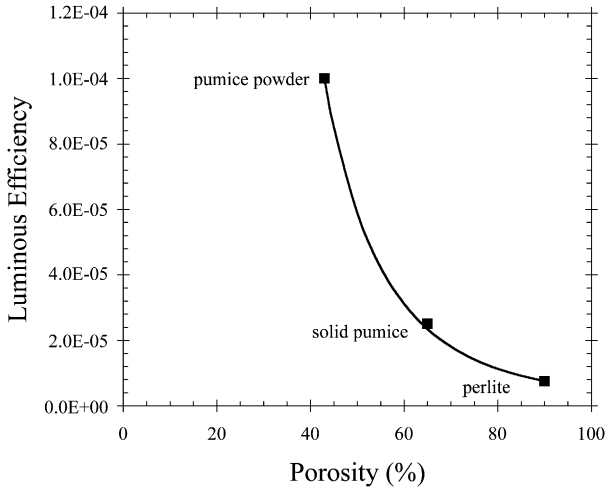

Fig. 7. Plot of the relationship between target porosity and luminous efficiency based on laboratory impacts into silicate targets (pumice powder, solid pumice, and perlite granules). The trendline represents the exponential relationship detailed in Eq. (4).

lower measured luminous efficiency. As the porosity increases from 43% to 90%, the luminous efficiency decreases by two orders of magnitude, from $\sim 10^{-4}$ to 10^{-6}.

Two major factors contribute to the lower photometric signal. First, as the projectile penetrates a highly-porous target, it encounters less mass per unit length along its path. Although shockwaves are known to heat porous materials to higher temperatures than non-porous materials (energy is irreversibly partitioned into heat through the compaction of pore space) (Love et al., 1993), there are initially few radiating sources produced near the surface, resulting in a lower initial photometric signal.

Second, a projectile impacting a highly-porous target penetrates much deeper before its energy and momentum are fully coupled to the target. The result is a long and narrow transient crater (Schultz et al., 2005). This deep penetration confines the heated material at early times, and prevents much of the initial light radiation from emerging above the surface and out of the transient crater. The result is a lower photometric signal due to there being fewer observable radiating sources.

The relationship between target porosity (ϕ) and luminous efficiency (η) can be defined quantitatively (Fig. 7). When examining the three targets of similar composition (pumice powder, solid pumice, perlite), the relationship follows an exponential function:

$$\eta = c_1 e^{c_2 \phi}, \tag{4}$$

where c_1 and c_2 represent constants. For the current laboratory experiments, the best fit to the data results in a value of $c_1 = 0.0011$ and $c_2 = -5.4$. It should be stressed that this relationship was derived using targets of similar particulate silicate composition, at the same impact angle, velocity, and projectile diameter. With assumptions, this relationship can be applied to the DI observations to estimate a porosity value for the Tempel 1 surface. This estimate is discussed in Section 4.1.

The effect of target volatile content on the impact flash was explored by using particulate dolomite, which is easily vaporizable under laboratory impact conditions. Volatiles in the target

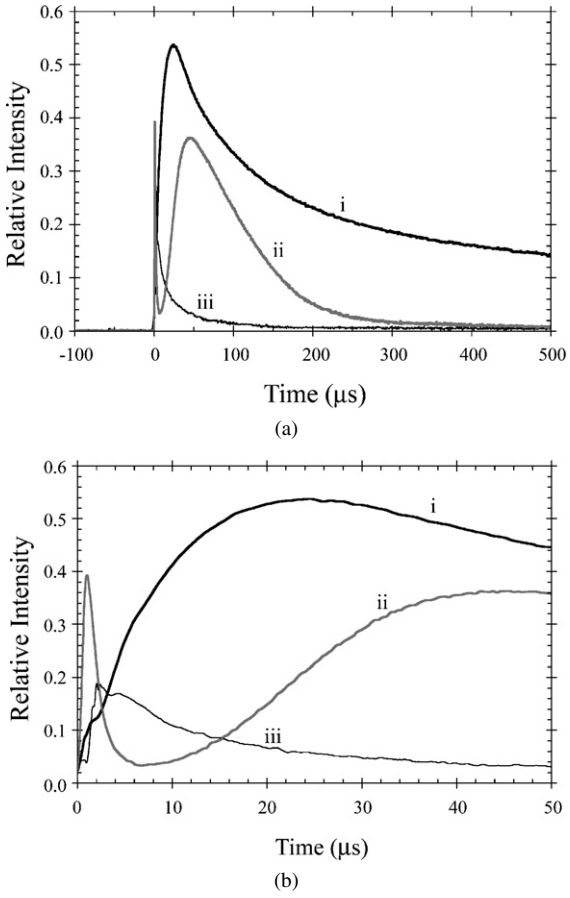

Fig. 8. Light intensity evolution of experimental impacts into silicate and carbonaceous targets: (i) pumice powder, (ii) sugar, and (iii) perlite granules. (a) The evolution from 0 to 500 μs. The pumice powder signal is the brightest and the longest. On impact, pumice particulates are heated and radiate as blackbodies while cooling. The sugar is vaporized on impact, later condensing into radiating particulates. The perlite target is porous, so much of the impact flash is hidden inside of the developing transient crater, resulting in a dim, short signal. (b) The evolution from 0 to 50 μs. The sugar target exhibits an evolution that is distinct from that of the pumice powder and the perlite.

(in the absence of an atmosphere) also decrease the brightness, duration, and luminous efficiency of the flash (Fig. 6). When volatiles are present, some of the impact energy is partitioned into vaporization and vapor expansion. Much of the emitted light is in the form of atomic and molecular emission lines at specific wavelengths, as opposed to a blackbody continuum (Eberhardy and Schultz, 2004); thus, the overall luminous efficiency is relatively low.

Impacts into targets containing carbon (sugar in the case of this study) yield flash evolutions distinct from those previously discussed. The resulting impact flash is of intermediate duration and brightness compared to flash signals from impacts into porous, volatile, and pumice powder targets (Fig. 8). For a target made completely of sugar, the impact flash begins with a bright intensity spike that fades and undergoes a secondary, delayed brightening.

Under laboratory conditions, sugar vaporizes on impact. This process is reflected in the in the rapid intensity drop after the first contact spike. As the vapor cloud cools, particles begin to condense from the vapor and begin to radiate as blackbodies. Because these particles condense over time, the secondary peak intensity is delayed and occurs at a much later time than the secondary peak intensity observed during impacts into pumice powder targets. The flash evolution undergoes an intermediate amount of change for impacts where the carbonaceous material is mixed into the target in smaller amounts. In contrast, the vaporization of a pumice target is minimal at laboratory-scale impact velocities; thus, heated pumice particulates continually radiate, resulting in a relatively continuous impact flash signal. The high emissivity of carbon and the possibility of secondary chemical reactions during condensation and recombination may also enhance the light flash (Schultz et al., 2007).

3.2. Target effects on impact flash spatial distribution

The use of a high-speed thermal imaging camera reveals the spatial distribution of self-luminous material for experimental impacts. Major differences in the distribution are observable when comparing impacts into targets of various porosities. Fig. 9a illustrates a side view of the setup for two experimental impacts. The experiments impacted 0.635 cm Pyrex spheres traveling at $\sim 5.50 \pm 0.03\ \mathrm{km\,s^{-1}}$ and at 30° angles (from the horizontal) into pumice powder under an ambient near-vacuum (0.64 mbar). Though otherwise identical, a projectile-thick layer of highly porous perlite granules overlaid the impact II pumice powder target. The target materials are the same as those described in Table 1. The camera was positioned above and slightly downrange of the impact point, and a 250 ns exposure was taken 20 μs after each impact.

Fig. 9b shows the resulting images taken by the thermal camera. The direction of impact and the approximate uprange/downrange location of the impact point are indicated in the figure. The experiments occurred in the dark, with no ambient light reaching the camera; therefore, the impacts generated all of the imaged light. Despite the thinness of the high-porosity layer, its presence had a significant effect on the resulting light distribution and intensity. The light generated by impact I is located entirely downrange of the impact point at the time of the exposure, and is confined to a well-defined area. The light generated by impact II extends not only downrange but also uprange of the impact point. The downrange component is fainter and much more diffuse than in impact I. Consequently, some of the emitting material may lie underneath the target surface at the interface between the perlite and the pumice powder layers. Schultz et al. (2005, 2007) also observed this phenomenon from a side view in quarterspace impact experiments.

The uprange portion of the impact II light signal is an uprange plume. Schultz (1996) and Schultz et al. (2007) address the general evolution and source of such plumes during impacts into highly porous targets. Because a projectile penetrates deeply into a high-porosity target, the early-generated vapor component is contained by the transient cavity, a phenomenon known as cavitation. A highly-collimated plume is directed back up the impactor-generated penetration funnel and travels uprange at a relatively high angle. Parts of the uprange plume are initially self-luminous, but because it is composed mostly of vapor phases, the plume remains relatively dim.

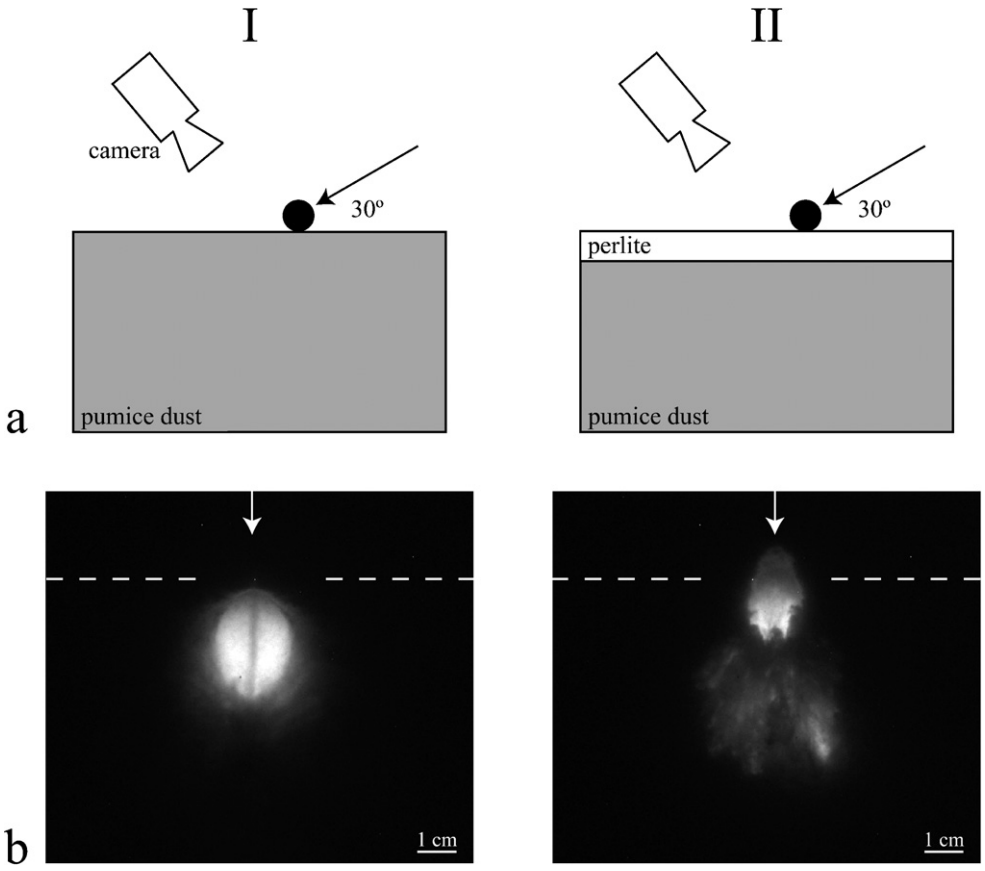

Fig. 9. The effect of a highly-porous surface layer on the spatial distribution of the impact flash. (a) Side views of the experimental setup of impacts I and II. In both cases, 0.635 cm Pyrex spheres impacted at ∼5.5 km s^{-1} at angles of 30°. The thermal imaging camera was located above and downrange of the impact point. Both targets were pumice powder, but a projectile-thick layer of highly-porous perlite granules overlaid the pumice for impact II. (b) The thermal imaging camera exposures: 250 ns exposures taken 20 μs after impact. The entire image is self-luminous material. The dashed line represents the uprange/downrange location of the point of impact, and the arrow represents the projected impactor trajectory. The addition of the high-porosity perlite layer caused major changes in the spatial distribution and exposure of the self-luminous components. The overall intensity was lower and much of the downrange component was more diffuse. All of the impact I self-luminous material was directed downrange of the impact point. In contrast, a portion of the impact II self-luminous material was directed uprange of the impact point in the form of a high-angle, uprange plume.

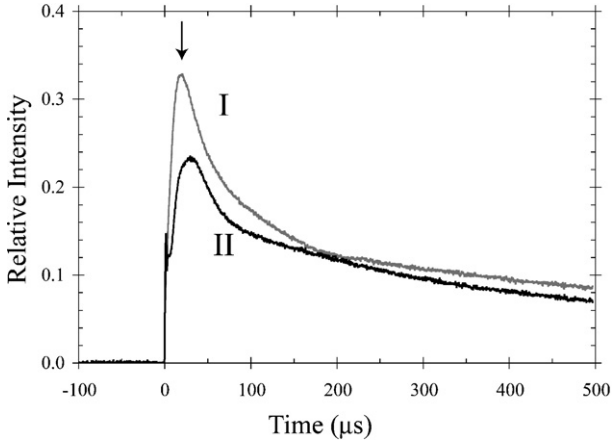

Fig. 10. The first 500 μs light intensity curves of impacts I (gray) and II (black) from Fig. 9. The signals look different at early times, and begin to converge at later times. There is an early-time spike in the impact II signal, followed by a brief intensity decrease before the eventual intensity peak. The arrow represents the time at which Fig. 9b images were taken.

Fig. 10 shows the light curves of impacts I and II out to 500 μs after impact, as recorded by a photodiode (sensitive to the 0.35–1.10 μm wavelength range). The photodiode was positioned above and slightly uprange of the impact point. Though the overall shapes of the curves are similar, there are observable details that differentiate the two. The impact II rise time (time to the peak) was ∼40% longer than that of impact I, and the impact II curve displays a visible change in decay rate at ∼70 μs. At later times (>250 μs), both light sources decayed at similar rates and had similar durations.

The cumulative light output for impact I was only ∼15% more than that for impact II. Since the porous layer was only as thick as the projectile, it initially affected the distribution and evolution of the light output at early times, but at later times the photometric decays were similar. If the porous layer were thicker, the light curve differences would be more pronounced and would persist longer into the recorded light signal.

4. Analysis and interpretations

The expanding downrange plume is known to be self-luminous because it passed by the spectrometer slit during the first HRI-IR exposure (∼200–250 ms after impact) as described

by A'Hearn et al. (2005). The continuum temperature of the downrange plume at this time was modeled to be ~850 K. The spectrometer also observed emission lines from vapor species with peak temperatures between 1000 and 2000 K. These observations indicate that the plume was composed of hot dust particles that were entrained in the downrange-moving and expanding vapor. The dust particles acted as blackbody radiators that cooled over time as the plume expanded. At earlier times (<200 ms after impact, before the plume passed by the slit) this dust component would have been even hotter. Melosh et al. (2006) modeled the dust component as a cloud of 150 μm diameter liquid silicate droplets that cooled from an initial temperature of ~3500 K.

Experimental oblique impacts produce a downrange-moving vapor plume that travels along the surface at a velocity comparable to the initial impact velocity while expanding hemispherically (Schultz et al., 2005; Schultz, 1996). On a three-dimensional body, this plume evolves into a spherically expanding cloud. The oblique view angle of the DI collision requires that the downrange plume velocity be corrected, taking into account the projection. Consequently, the observed downrange speed of ~6 km s^{-1} for the leading edge becomes ~12 km s^{-1}, assuming a 30° impact angle.

4.1. Luminous efficiency and duration

First-order predictions for the brightness and duration of the DI flash were based on extrapolations from laboratory impacts (Schultz et al., 2005; Ernst and Schultz, 2005). For reference, the predictions incorporated a simplified assumption of a pumice powder-like target (no volatiles, 43% porosity), although target porosity and volatile content were observed to also affect the duration and intensity of the impact flash. The flash was predicted to last at least 0.06 s (one MRI exposure frame), with the prospect of lasting 10–50 times longer if the Tempel 1 surface is particulate and silicate-rich. The predicted cumulative luminous energy output under these assumed conditions was ~15 MJ, thereby resulting in a predicted luminous efficiency (in the MRI wavelength range) of the DI flash of $\sim 8 \times 10^{-4}$.

The actual luminous efficiency of the DI flash was calculated by integrating the total light output over time of the self-luminous components of the impact-induced light signal. Simple linear interpolation between frames accounted for the brief time gaps. Due to the saturated images, the calculated luminous efficiency value must be considered a lower limit. However, the inclusion of the spill over pixel values into the total luminous energy output reasonably compensates for the saturation and provides a closer estimate of the actual brightness. The calculated luminous efficiency based on the MRI images was $\sim 7 \times 10^{-5}$, an order of magnitude less than predictions. This difference most likely results from the use of silicate powder as the reference target, which was not meant to represent the Tempel 1 surface. The actual light output of an impact is affected by factors that were purposely not taken into account for the prediction, such as target porosity, particle emissivity, volatile content, strength, and optical depth. Consequently, the difference between predictions and observations provides useful information about the nature of the surface materials of Tempel 1 at the impact site. The dimmer than expected luminous efficiency implies that the surface is highly porous, contains volatiles, or a combination of the two.

Although the predicted and measured values of the total luminous output differed, the flash duration was actually consistent with the lower bound of expectations for a long-lasting flash (Schultz et al., 2005). Laboratory impacts into highly porous (perlite) and highly volatile (particulate dolomite) targets demonstrate that the impact flash is much shorter than the flash from impacts into pumice powder. Any porosity or volatiles on the surface of Tempel 1 would drastically shorten the duration of the self-luminous component, perhaps even confining it to one MRI exposure. Since the signal was significantly longer than one exposure, another factor must be acting to lengthen the signal duration. Carbon-based compounds (CH-X) are known to exist on or near the surface of Tempel 1 based on spectral measurements during the impact event (A'Hearn et al., 2005; Sunshine et al., 2007). These compounds may contribute to the reduced luminous efficiency yet prolonged duration of the flash due to their high emissivity and the possible evolution of back reactions within the vapor plume.

The relationship between target porosity and luminous efficiency [Eq. (4)] can be scaled to DI conditions by making a few assumptions. First, it is assumed that the exponential constant (c_2) is the same at all scales. Second, c_1 is calculated to be 0.0082 based on the predicted DI luminous efficiency value of 8×10^{-4}, assuming a 43% surface porosity and a silicate target (Schultz et al., 2005). Plugging both this new c_1 and the DI luminous efficiency calculated here (a lower limit of 7×10^{-5}) into Eq. (4) yields an 88% porosity value for the upper surface of the comet. For a silicate surface composition (2.2 g cm^{-3}), this corresponds to a surface density of 0.26 g cm^{-3}. If the actual luminous efficiency were twice as high as the calculated lower limit (to try to compensate for saturation effects), the values would be 75% porosity and 0.55 g cm^{-3}.

Because of the assumptions made and the factors not taken into account, especially target composition, these calculations must be considered an exercise. Various phenomena observed in the DI event, however, are similar to those seen in laboratory impacts into targets with porosities in this range (Schultz et al., 2007). A'Hearn et al. (2005) place a rough estimate of 0.6 g cm^{-3} on the bulk density of the Tempel 1 nucleus. This value is close to those calculated here, and it is reasonable to believe the surface density of the nucleus would be lower than the bulk density; therefore, the results of this exercise have some merit.

4.2. Source movement

The faint "first light" appears uprange of the projected impact point (Fig. 5). In subsequent images, the center of brightness of the impact flash moves in a downrange direction, traveling closer to the impact point. This motion indicates that the first light represents a self-luminous component uprange from the developing crater.

The view angle of the impact was 3.3° off of the impactor trajectory, thus any early light source inside of the transient crater would appear along the projected trajectory. The first light appears slightly off-axis from the trajectory, indicating that the light source rose above the surface at an angle higher than the impact angle. Consequently, the first light does not represent the path of the projectile through an upper surface.

The apparent motion and the off-trajectory position of the first light are consistent with the existence of an uprange plume created by the containment and redirection of vapor by a deep and narrow transient crater. The self-luminous nature of the uprange plume is mainly due to atomic and molecular emission lines. This light component fades quickly due to a low affected mass and the lack of significant thermal emissions. Predictions made by Schultz et al. (2005), observations of the DI event made by the Hubble Space Telescope (Feldman et al., 2007), and data from the DI flyby spacecraft (Schultz et al., 2007) support the existence of a long-lasting, uprange plume. Based on results from laboratory impact experiments, the existence of an uprange plume implies that the surface of Tempel 1 is highly porous. This conclusion is consistent with those derived from the photometric characteristics.

4.3. Summary

The initial faint flash followed by the delayed saturated flash farther downrange can be explained by an oblique impact into a low-density (0.2 to 0.5 $g\,cm^{-3}$) particulate target as documented in laboratory experiments. In this scenario, the first light is a plume of radiating dust and gas directed uprange of the initial penetration funnel due to cavitation. In laboratory experiments, this initial plume is highly collimated and is relatively faint due to the low affected mass (caused by high target porosity) and/or the dominance of vapor phases (absence of significant thermal radiation) (Ernst and Schultz, 2005). The apparent movement of the early flash is due to the evolution of this uprange plume and the subsequent opening of the transient crater.

As the transient crater develops, the initial penetration funnel opens, exposing the once-hidden, shock-heated material at the surface as it emerges and moves downrange of the impact point (corresponding to frames D and E from Fig. 2) while retaining a substantial fraction of the initial impact velocity (Schultz, 1996; Ernst and Schultz, 2003). Hot, radiating particulates entrained in this vapor plume move and expand downrange of the impact point. Vapor expansion adds an additional velocity component to the plume's leading edge. Tracing the downrange plume back to the moment of emergence from the surface indicates that this velocity component should appear ∼100 ms after the first light. The subsequent delay in the bright flash can be interpreted as the combination of the initial rapid expansion, the time before the opening of the penetration funnel, obscuration during projectile entry, and the initial absence of thermal radiation due to the early dominance of emission lines (see Schultz et al., 2007). Such a scenario was outlined as a predicted result of a highly porous Tempel 1 nucleus in Schultz et al. (2005). A highly porous surface layer is also supported by the analyses performed by Schultz et al. (2007) and Richardson and Melosh (2006).

Spectral data and observations of the post-impact downrange vapor plume are evidence that volatiles exist on or near the Tempel 1 surface (A'Hearn et al., 2005; Sunshine et al., 2006). Though their presence may contribute to lowering the luminous efficiency of the DI collision, it cannot explain all of the observed phenomena; volatiles alone will not produce an uprange plume. The surface also must contain significant quantities of "dust" (or condensates) to create the thermal signal entrained in the downrange vapor plume, some of which could be silicate in nature, and some of which could be condensed, high-emissivity carbon. Both silicate dust and carbonaceous material were detected in the initial self-luminous plume by the IR spectrometer (Sunshine et al., 2007; A'Hearn et al., 2005).

5. Conclusions

The Deep Impact flyby spacecraft successfully recorded the light flash produced by the impactor's collision with Comet Tempel 1. The "flash" persisted through multiple MRI exposures, which enabled the analysis of the flash evolution through time. The photometric and spatial evolutions of the DI flash provide independent constraints on the nature of the Tempel 1 surface through comparisons with laboratory impact flash data.

The DI impact flash consisted of three self-luminous components: the "first light," the saturated central flash, and the downrange plume. The "first light" appeared uprange of the projected point of impact. The light intensity then faded briefly before undergoing a second brightening at a position closer to the impact point. This central self-luminous component quickly and dramatically brightened, which resulted in detector saturation. A downrange-moving plume then emerged from the impact site, consisting of vapor and entrained, radiating dust particles. The combined luminous efficiency of these three components was lower than predictions based on simplified laboratory experiments using silicate powder; however, the duration was comparable to predictions. The difference between the predictions and observations indicates the effect of high porosity and the presence of volatiles that suppress the luminous efficiency.

The photometric and spatial evolutions of the DI first light are consistent with the existence of an uprange plume directed up and out of the penetration funnel due to cavitation. The delayed brightening results from the emergence of heated material with the opening of the transient crater. Based on comparisons with laboratory impact flash studies, these observations and the low luminous efficiency are consistent with an under-dense (porous) target surface.

Volatiles exist on the Tempel 1 surface, as evidenced by the existence of the downrange plume. This plume entrained blackbody-radiating particles and translated them downrange away from the impact site. These entrained particles allowed the vapor plume to be easily detected by the MRI camera. The existence of a vapor plume is consistent with results from the MRI-IR spectrometer.

Though the DI flash was dimmer than predicted, its duration was on the long side of expectations, thereby suggesting an ad-

ditional target component. The presence of carbon compounds could account for the long duration, since carbon compounds vaporize and condense at lower temperatures than silicates. The condensation of carbon compounds in the downrange plume would create new particulate radiators at later times, thus resulting in a long decay time. Future experimental studies will be able to quantify such effects.

The impact flash is an effective remote sensing tool. Details of the Tempel 1 surface were independently constrained by photometry alone, and these constraints agree with conclusions drawn through other means (e.g., spectrometry, ejecta behavior). Laboratory experiments are critical to understand the underlying processes that caused the observed photometric and spatial evolutions of the light flash.

Acknowledgments

We are grateful to D. Holt, D. Bowling, and R. Smythe at the NASA Ames Vertical Gun Range for their assistance and technical expertise. We thank M.F. A'Hearn for his valuable comments. We also thank N. Artemieva and an anonymous referee for their constructive reviews, which have improved the quality of this manuscript. This research was supported by the NASA Discovery Program Deep Impact mission (NASW-00004) and by the NASA Graduate Student Researchers Program (04-6011H).

References

A'Hearn, M.F., and 32 colleagues, 2005. Deep Impact: Excavating Comet Tempel 1. Science 310, 258–264.

Bellot Rubio, L.R., Ortiz, J.L., Sada, P.V., 2000a. Luminous efficiency in hypervelocity impacts from the 1999 lunar Leonids. Astrophys. J. 542, L65–L68.

Bellot Rubio, L.R., Ortiz, J.L., Sada, P.V., 2000b. Observation and interpretation of meteoroid impact flashes on the Moon. Earth Moon Planets 82–83, 575–598.

Eberhardy, C.A., Schultz, P.H., 2004. Probing impact-generated vapor plumes. Proc. Lunar Sci. Conf. 35. Abstract 1855.

Eichhorn, G., 1976. Analysis of the hypervelocity impact process from impact flash measurements. Planet. Space Sci. 24, 771–781.

Ernst, C.M., Schultz, P.H., 2002. Effect of velocity and angle on light intensity generated by hypervelocity impacts. Proc. Lunar Sci. Conf. 33. Abstract 1782.

Ernst, C.M., Schultz, P.H., 2003. Effect of initial conditions on impact flash decay. Proc. Lunar Sci. Conf. 34. Abstract 2020.

Ernst, C.M., Schultz, P.H., 2004. Early-time temperature evolution of the impact flash and beyond. Proc. Lunar Sci. Conf. 35. Abstract 1721.

Ernst, C.M., Schultz, P.H., 2005. Investigations of the luminous energy and luminous efficiency of experimental impacts into particulate targets. Proc. Lunar Sci. Conf. 36. Abstract 1475.

Feldman, P.D., McCandliss, S.R., Route, M., Weaver, H.A., A'Hearn, M.F., Belton, M.J.S., Meech, K.J., 2007. Hubble Space Telescope observations of Comet 9P/Tempel 1 during the Deep Impact encounter. Icarus 187, 113–122.

Gehring, J.W., Warnica, R.L., 1963. An investigation of the phenomena of impact flash and its potential use as a hit detection and target discrimination technique. Symposium on Hypervelocity Impact 6, 627–681.

Hampton, D.L., Baer, J.W., Huisjen, M.A., Varner, C.C., Delamere, A., Wellnitz, D.D., A'Hearn, M.F., Klaasen, K.P., 2005. An overview of the instrument suite for the Deep Impact mission. Space Sci. Rev. 117, 43–93.

Kadono, T., Fujiwara, A., 1996. Observation of expanding vapor cloud generated by hypervelocity impact. J. Geophys. Res. 101 (E11), 26097–26109.

Klaasen, K.P., Carcich, B., Carcich, G., Grayzeck, E.J., McLaughlin, S., 2005. Deep Impact: The anticipated flight data. Space Sci. Rev. 117, 335–372.

Love, S.G., Horz, F., Brownlee, D.E., 1993. Target porosity effects in impact cratering and collisional disruption. Icarus 105, 216–224.

Melosh, H.J., and Deep Impact Team, 2006. Deep Impact: The first second. Proc. Lunar Sci. Conf. 37. Abstract 1165.

Ortiz, J.L., Sada, P.V., Bellot Rubio, L.R., Aceituno, F.J., Aceituno, J., Gutierrez, P.J., Thiele, U., 2000. Optical detection of meteoroidal impacts on the Moon. Nature 405, 921–923.

Ortiz, J.L., Quesada, J.A., Aceituno, J., Aceituno, F.J., Bellot Rubio, L.R., 2002. Observation and interpretation of Leonid impact flashes on the Moon in 2001. Astrophys. J. 576, 567–573.

Richardson, J.E., Melosh, H.J., 2006. Modeling the ballistic behavior of solid ejecta from the Deep Impact cratering event. Proc. Lunar Sci. Conf. 37. Abstract 1836.

Schultz, P.H., 1996. Effect of impact angle on vaporization. J. Geophys. Res. 101 (E9), 21117–21136.

Schultz, P.H., Gault, D.E., 1990. Prolonged global catastrophes from oblique impacts. In: Sharpton, V.L., Ward, P.D. (Eds.), Global Catastrophes in Earth History: An Interdisciplinary Conference on Impacts, Volcanism, and Mass Mortality. GSA Special Paper 247. Geological Society of America, Boulder, pp. 239–261.

Schultz, P.H., Ernst, C.M., Anderson, J.L.B., 2005. Expectations for crater size and photometric evolution from the Deep Impact collision. Space Sci. Rev. 117, 207–239.

Schultz, P.H., Sugita, S., Eberhardy, C.A., Ernst, C.M., 2006. The role of ricochet in impact vaporization. Int. J. Impact Eng. 33, 771–780.

Schultz, P.H., Eberhardy, C.A., Ernst, C.M., Sunshine, J.M., A'Hearn, M.F., 2007. The Deep Impact oblique cratering experiment. Icarus 190, 295–333.

Sunshine, J.M., and 22 colleagues, 2006. Exposed water ice deposits on the surface of Comet 9P/Tempel 1. Science 311, 1453–1455.

Sunshine, J.M., Groussin, O., Schultz, P.H., A'Hearn, M.F., Feaga, L.M., Farnham, T.L., Klassen, K.P., 2007. The distribution of water ice in the interior of Comet Tempel 1. Icarus 190, 284–294.

Thomas, P.C., and 14 colleagues, 2007. The shape, topography, and geology of Tempel 1 from Deep Impact observations. Icarus 187, 4–15.

Yanagisawa, M., Kisaichi, N., 2002. Lightcurves of 1999 Leonid impact flashes on the Moon. Icarus 159, 31–38.

Zahnle, K., MacLow, M.M., 1995. A simple model for the light curve generated by a Shoemaker–Levy 9 impact. J. Geophys. Res. 100 (E8), 16885–16894.